38th International Electric Vehicle Symposium and Exhibition (EVS38) Göteborg, Sweden, June 15-18, 2025

Comparison of waveform distortion from five different EVs charging on a Low-Voltage grid

Manav Giri[1], Sarah Rönnberg[2]

[1]*Luleå University of technology, Forskargatan 1, Skellefteå, manav.giri@ltu.se*

[2]*sarah.ronnberg@ltu.se*

Executive Summary

This paper presents an evaluation of waveform distortion resulting from the charging of five different electric vehicles (EVs) on a low-voltage distribution network with variable cable impedance, achieved by adjusting cable lengths. The influence of cable impedance on harmonic, interharmonic, and supraharmonic emission is modeled and analyzed. Additionally, the role of background supraharmonic distortion is investigated to identify potential contributing sources. Based on detailed measurements, insights into the modeling of EV-induced waveform distortion are derived and discussed.

Keywords: Electric Vehicles, Electromagnetic Compatibility, Measuring Methods and Equipment, Modelling Simulation, AC Charging technology.

1 Introduction

Achieving net-zero emissions by 2050 requires a complete phase-out of new internal combustion engine (ICE) vehicle sales by 2035 [1]. Fig.1 shows the electric vehicles (EV) and Plug-in Hybrid Electric Vehicle (PHEV) sales trend in Sweden from 2005 to 2024, highlighting their increasing share of total passenger car sales, reaching approximately 57% in 2023 [2].

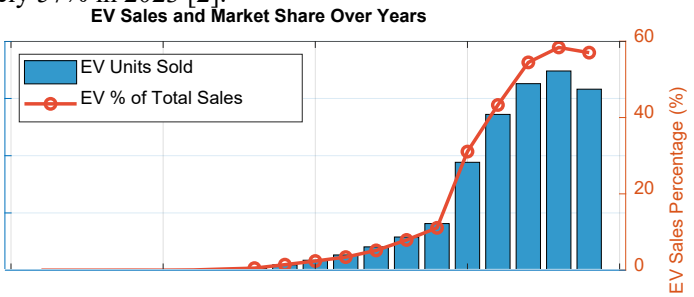

Figure 1: Trend of EV sales in Sweden from 2005 to 2024 along with the percentage of BEVs and PHEVs as a percentage of total passenger car sales in Sweden[2]

The growing adoption of EVs in low-voltage (LV) distribution grids is contributing to increased waveform distortion [3],[4]. This distortion refers to deviations of the voltage waveform from its ideal sinusoidal shape [5] (ch1, Pg.5) and can result from harmonic (integer multiples of grid frequency), interharmonic (non-integer multiples), and supraharmonic (2–150 kHz) components, which are introduced by non-linear loads such as EV chargers. While harmonic [3], [6], [7], [8] and supraharmonic emissions from electric vehicles [9], [10], [11], [12] have been studied, interharmonic emissions have received limited attention. To the best of the authors' knowledge, no comparative analysis across interharmonic, harmonic, and supraharmonic emissions exists, despite the risk that interharmonic limits may be exceeded first during large-scale EV charging.

The organization and contribution of this paper are as follows. Section 2 explains the measurement setup, and the regulatory and proposed emission limits used in the paper are presented. Section 3 investigates harmonic, interharmonic, and supraharmonic emissions from five commercially available EVs in Sweden and compares emissions against regulatory limits in varied cable impedance conditions. Section 4 further examines the influence of cable impedance with a proposed model and compares the model predictions against the

measurements. In Section 5, the impact of supraharmonic background distortion on supraharmonic emission is discussed with a possible explanation of some of the additional spectral components observed in the emission spectra. It introduces a light quasi-peak (QP) method for supraharmonic assessment. The study also analyzes how background voltage distortion affects these emissions.

2 Measurement Setup

Fig.2 shows the measurement setup. The Thevenin impedance at POC-2 comprises the transformer's short-circuit impedance, leakage reactance, winding resistance, and variable cable lengths between points A and B after the PCC. Contributions from other loads are neglected. Table 1 lists the calculated Thevenin impedances for different cable lengths.

Table 1: Thevenin impedance (50 Hz) used during the EV charging in Pehr Högström laboratory.

Network Thevenin Impedance	Z1	Z2	Z3
Unit (Ohms)	0.3546 + j0.0285	1.3153 +j0.0693	1.8562 + j 0.0924
Cable Length (m)	1	180	281

Measurements were conducted at POC-1 using an IEC 61000-4-30 Class A Power Quality Analyzer, and at POC-2 using waveform recorders. Five commercially available EVs in Sweden were tested at the Pehr Högström Laboratory using electric vehicle supply equipment (EVSE) configured for 11 kW (three-phase) or 7.2 kW (single-phase) output, with a maximum phase current of 16 A. Table 2 summarizes the tested EVs, charging durations, corresponding Thevenin impedances, and measurement instruments.

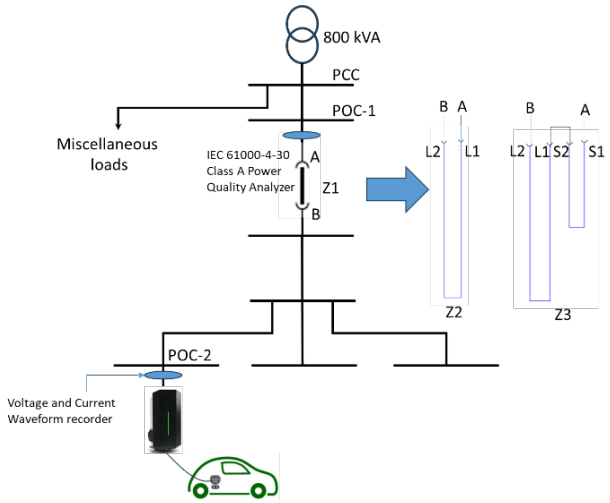

Figure 2: Measurement setup at Pehr Högström Laboratory. The setup enables the possibility of changing the cable length between POC1 and POC2.

The waveform recorders are configured to record 500 ms of voltage and current waveforms every minute. The Yokogawa DL850 waveform recorder comprises a 12-bit ADC for recording voltage waveforms at 1 MHz and a current waveform with a 16-bit ADC at 1 MHz. The DEWEsoft Sirius waveform recorder uses 16-bit ADCs to record both voltage and current waveforms and to sample the waveforms at 500 kHz. The noise floor for the voltage and current harmonics based on the channel settings for the voltage and current channels is also identified in Table 2

A typical EV charging session includes one or more constant current (CC) stages, followed by a constant voltage (CV) stage, depending on the battery state of charge (SoC). For EV1, charging occurs in a CC stage up to 80% SoC, then transitions to a lower current CC2 stage until charging ends. EV2 charges in CC stage up to 90% SoC, after which it enters the CV stage, where charging current decreases exponentially. These current variations reflect manufacturer-defined responses to SoC under IEC 61851-1 [13] Mode 3 charging. The configured EVSE's power rating and charging infrastructure limit the maximum current, including protective devices and cabling. Charging stages observed during each session are detailed in Table 2.

2.1 Compatibility and Emission Limits

EV waveform distortion during Mode 3 charging is governed by IEC 61851-21-1 [14], which references IEC 61000-3-2(<16 A) [15] and IEC 61000-3-12 (16–75 A) 23[16] to maintain voltage distortion within IEC 61000-2-2 [17] compatibility levels. However, IEC 61851-21-1 does not specify limits for interharmonic or supraharmonic emissions. To address this gap, interharmonic current limits used in this study (Fig. 3a) follow the methodology in [18], [19], which also outlines a procedure for supraharmonic limits in the 2–9 kHz range.

This is extended to 9–150 kHz, assuming unity resonance and splitting factors, resulting in the emission envelope shown in Fig. 3(b).

Table 2: Details of the EVs, measurement window, and network impedances utilized during the measurement exercise at the Per Högstrom laboratory

#	Waveform Recorder	Voltage Harmonics Least count (mV)	Current Harmonics Least count (mA)	Peak Mode 2/3 Charge Power	Observation Window (minutes)	Charging stages observed	Network Impedance for measurements
EV1	Yokagawa DL850	5	0.4	3 Phase 11 kW	288 (Z1) 324 (Z2) 273 (Z3)	CC1,CC2	Z1,Z2,Z3
EV2	Yokagawa DL850	5	0.4	3-Phase 11 kW	357 (Z2) 395 (Z3)	CC/CV	Z2,Z3
EV3	Yokagawa DL850	5	0.4	1-Phase 2.2 kW	407	CC	Z2
EV4	Yokagawa DL850	5	0.4	1 Phase 3.3 kW	339	CC	Z2
EV5	DEWEsoft Sirius	70.8e-3	0.5	1 Phase 2.4 kW	59	CC	Z1

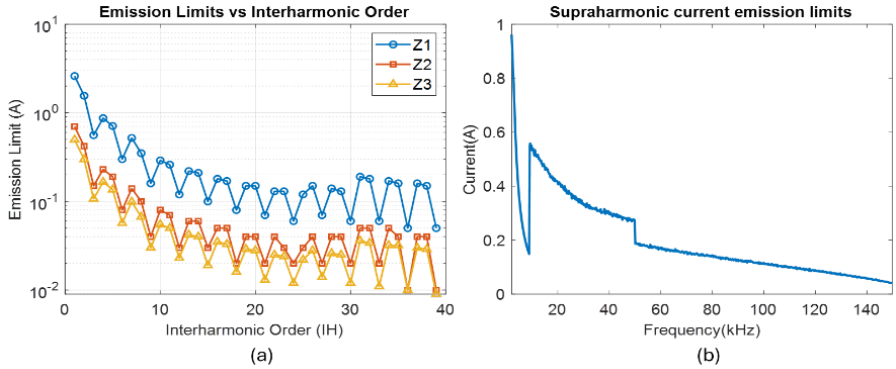

Figure 3: Emission limits for EV charging based on procedure identified in [18], [19].(a) Interharmonic current emissions (b) Supraharmonic current emissions.

3 Comparative analysis of Conducted Emissions from an EV charging session

A comparative analysis of conducted emissions was carried out across five different EV models to better understand the electromagnetic behavior of electric vehicles during charging. This section presents the key findings from these measurements, highlighting differences in spectral content, interharmonic components, and statistical trends observed in the current signals. Examining representative metrics such as maximum emission levels, interharmonic distribution, and statistical variation aims to identify common patterns and unique characteristics among the EVs under test.

3.1 Interharmonic emissions

To evaluate interharmonic current emissions, the analysis follows the interharmonic subgrouping methodology defined in IEC 61000-4-7 [20]. Only the interharmonic currents are reported in this subsection, as the measured interharmonic voltages are below the threshold of 0.1% and hence can be ignored as suggested in IEC 61000-3-14 [21]. The interharmonic current emissions for EVs, along with the network impedance on which the measurements are undertaken (Table 2), are reported in Fig.4. The current emissions are compared against the emission limits reported in Fig. 3(a).

For EVs 1 and 2 equipped with three-phase onboard chargers, only the maximum value among the 95th percentile and mean of the three phases is reported. As a result, any phase-to-phase diversity in emissions arising from variations in background voltage distortion, fundamental voltage levels, or differences in the grid's Thevenin impedance at the point of connection is not captured in this analysis. Consequently, the potential asymmetries and localized effects unique to each phase during three-phase EV charging are overlooked. Additionally, in this case the change in emissions during the different charging stages (CC and CV) amongst the EVs is ignored for interharmonic current emissions.

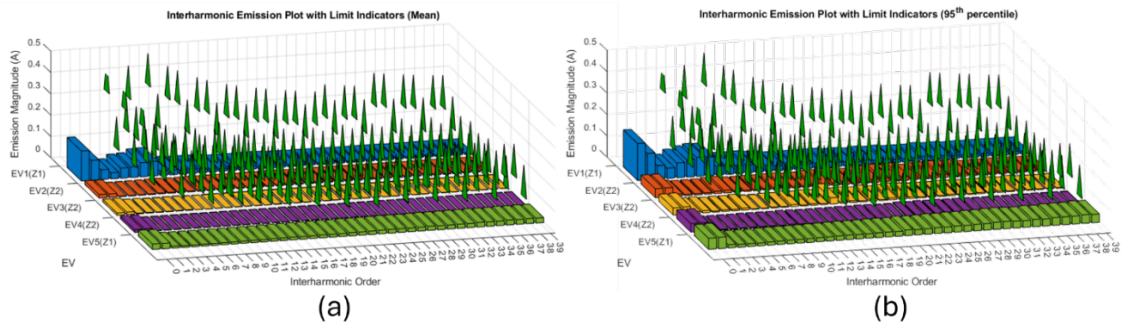

Figure 4: Interharmonic current emissions from EVs 1 to 5 compared against derived emission limits. Limits identified in the plot with green color indicate no violation (a) Statistical mean (b) 95th Percentile

Based on the reported results, no emission limit violations were observed during single EV charging on the low-voltage (LV) grid. Among the tested vehicles, EV1 exhibited the highest interharmonic emissions, prompting a more detailed analysis. Specifically, the interharmonic current emissions of EV1 were evaluated for different cable lengths and compared against the emission limits illustrated in Fig. 3(a). The mean values of these emissions are presented in Fig. 5(a), while the 95th percentile values are shown in Fig. 5(b). Notably, emission limit violations are seen in Fig. 5(b) for interharmonic orders 6, 12, 18, 21, 24, and 39 when connected through network impedance Z3. Further analysis on the difference in emissions for different cable lengths will be taken up in Section 6.

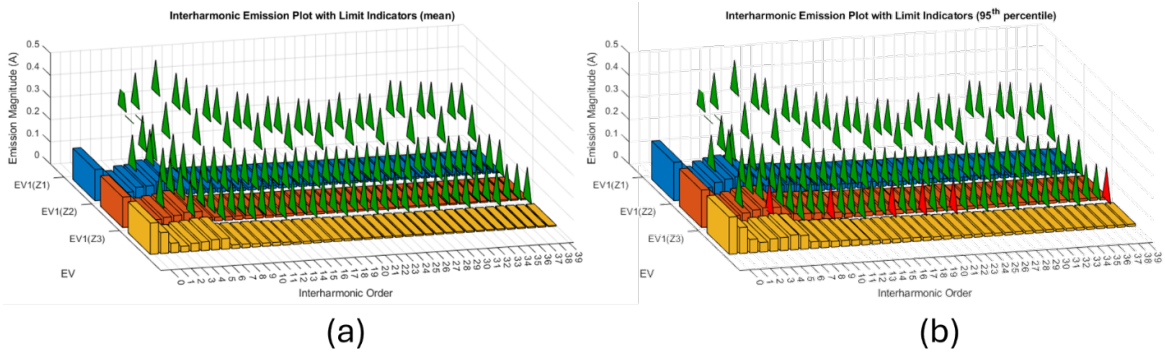

Figure 5: Interharmonic current emissions from EV 1 compared against derived emission limits. Limits shown in green indicate compliance; red indicates a violation. (a) Statistical mean (b) 95th Percentile

4.2 Harmonic emissions

To evaluate the harmonic behavior of electric vehicles during charging, a detailed analysis of current and voltage distortion was conducted using time-aggregated measurements. Similar to the analysis in Section 4.1, the maximum value among the 99th percentile and mean of the three phases is reported. Figures 6(a) and 6(b) present the 99th percentile harmonic current and voltage distortion levels, aggregated over 3-second intervals, from the EV charging sessions listed in Table 2. Each row in the bar-plots corresponds to a distinct measurement instance captured during the primary stage of charging. EV1 was tested in two charging stages: CC1, with a fundamental current of 16 A, and CC2, with a reduced current of 5 A. EV2, when connected to grid impedance Z3, entered a constant voltage (CV) stage while charging to 100% state of charge (SoC). The charging session for EV2 was terminated when the fundamental current dropped below 5 A. In contrast, EV3, EV4, and EV5 each exhibited only a single CC stage. For consistency, only the primary charging stage is considered for all EVs in the analysis in Fig. 6.

To emphasize the most significant findings, only those harmonic orders where EV1 exhibited current emission limit violations namely orders 5, 7, 11, 13, 17, 19, 21, 23, 25, and 31 when charging on grid impedance Z1 are presented. These harmonics are also shown for EV2 through EV5 to provide comparative context, although each EV was tested under different grid impedance conditions (see Table 2). In addition to EV1, EV2 also exhibited violations when tested on Z2 and Z3. Specifically, violations were observed on harmonics 13, 17, 19, 21, 23, 25, and 31 on Z2. EV3, EV4, and EV5 did not show any current emission limit violations across the tested harmonics. Furthermore, EV5 exceeded the voltage compatibility limit for harmonic 15, as defined i[17]. Accordingly, current emissions at harmonic 15 are included for all EVs to assess their contribution to voltage distortion. The corresponding harmonic voltage distortion levels are presented in Figure 6(b).

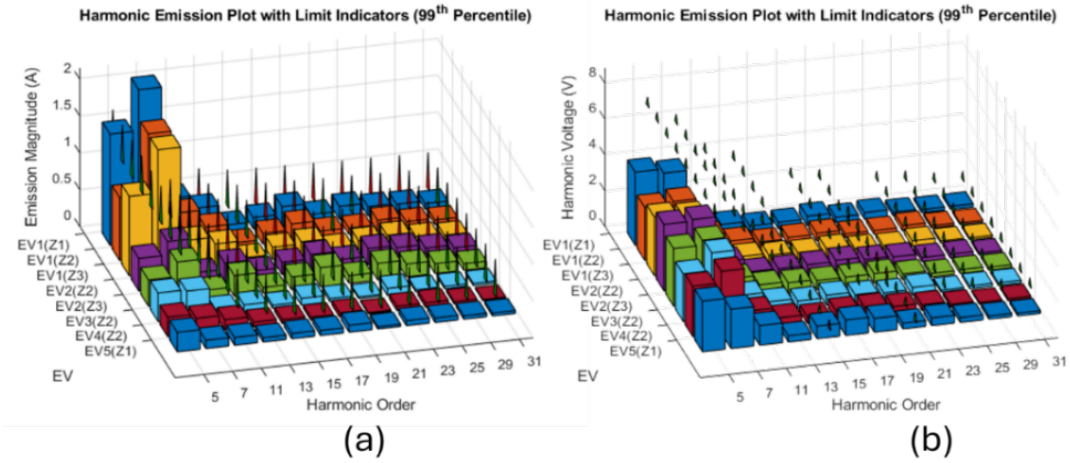

Figure 6: Three-second aggregated 99th percentile harmonic emissions from EVs 1–5 under varying grid impedances, compared to emission limits in Stage 1: (a) harmonic currents, (b) harmonic voltages. Green limit indicators (triangle on top of bar chart) indicate compliance; red indicates violation.

Figures 7(a) and 7(b) present the harmonic current emissions and corresponding voltage distortion during the CC2 stage of EV1 and the CV stage of EV2. For EV1, when charging on grid impedance Z1, emission limit violations persist, though in this stage, violations at harmonic orders 21 and 31 are no longer observed. For EV2, during the CV stage on Z3, violations are observed at harmonic orders 13, 17, 19, 23, 25, 29, and 31.

A comparative analysis of the emission magnitude differences across charging stages and grid impedance conditions is provided in Section 5, highlighting the influence of both charging mode and network characteristics on harmonic behavior

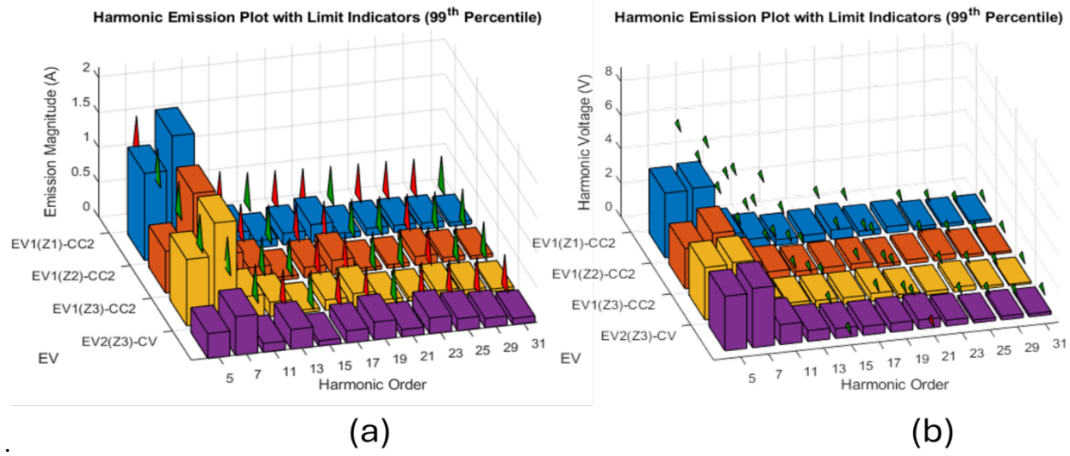

Figure 7: Three-second aggregated 99th percentile harmonic emissions from EVs 1–5 under varying grid impedances, compared to emission limits in Stage 2: (a) harmonic currents, (b) harmonic voltages. Green indicators indicate compliance; red indicates violation.

The observed emission limit violations can, in part, be attributed to the presence of existing background voltage distortion, which in these cases does not comply with the permissible limits outlined in IEC 61000-3-2[15]. These results underscore the fact that devices tested in controlled laboratory environments (using a Line Impedance Stabilization Network (LISN) and voltage distortion levels within the [15][15] defined thresholds) may exhibit substantially different emission behavior when tested under real-world grid conditions. In this context, resonance phenomena within the Frequency Dependent Network Impedance (FDNI) are not considered the primary cause of the observed violations, as the corresponding harmonic voltage levels remain within compatibility limits, and the emission magnitudes are not excessively high. This highlights the role of pre-existing grid distortion in influencing test outcomes and reinforces the importance of contextual field measurements in electromagnetic compatibility (EMC) assessments.

4.3 Supraharmonic emissions

The emissions in the frequency range 2-150 kHz are compared in this section. For comparison, in Fig.8, a comparison of the emissions (both voltage and current) as a percentage of the limit is presented. A logarithmic color scale is used to improve visibility of lower emission levels across all EVs. A violation of the emission

limit is defined as any instance where the measured emission exceeds 100% of the specified limit. In the logarithmic representation used in the heatmap plots, this corresponds to values where $\log_{10}$(% of limit) is greater than 2, since $\log_{10}(100) = 2$. Values exceeding this threshold indicate that the emission has surpassed the permissible limit and thus represents non-compliant behavior under the applicable limits. Similar to the previous section, for three-phase charging scenarios involving EV1 and EV2, the analysis considers the maximum of the 95th percentile values across the three phases, evaluated over the frequency range of 2–150 kHz. In Figure 8, only the emissions during the primary constant current (CC) stage are analyzed, ensuring a consistent basis for comparison across the measured sessions and capturing the worst-case emission behavior per measurement instance. Figure 8(a) shows the supraharmonic current limits as a percentage of the limits identified in Fig.3(b). Fig 8(b) shows the corresponding supraharmonic voltages. The following observations are made from Fig.8(a) and 8(b)

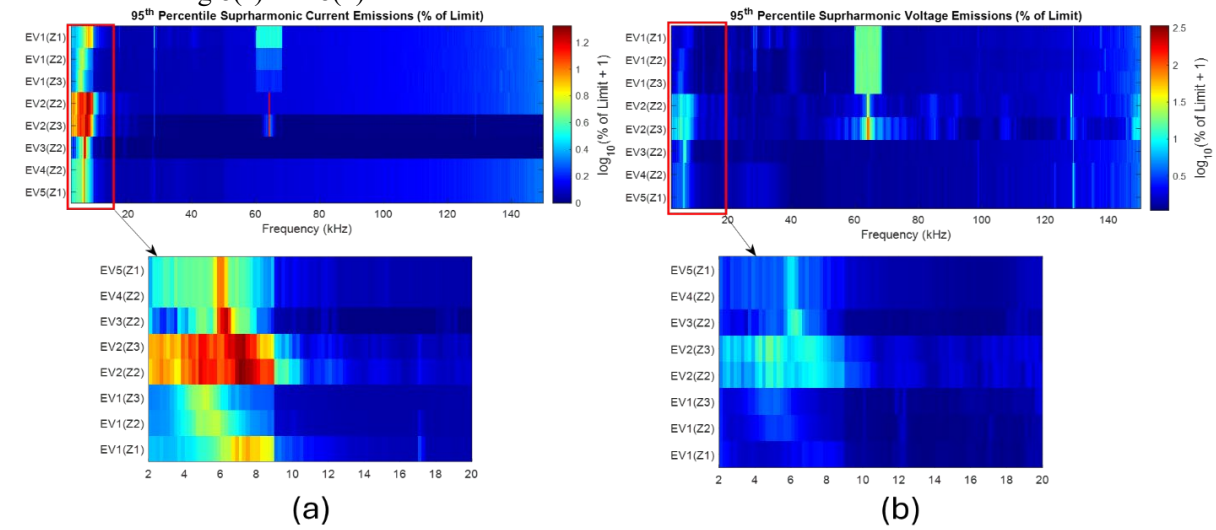

Figure 8: Heatmap of 95th percentile emissions expressed as % of the limit for EVs 1 to 5 for different grid impedances (a) Supraharmonic currents as a percentage of limits (b) Supraharmonic voltage as a percentage of limits..

- The emissions from all EVs can be broadly categorized into three distinct frequency segments: (i) emissions in the range of 2–10 kHz, (ii) a prominent emission component centered around 28 kHz, and (iii) emissions within the range of 60–70 kHz. These spectral characteristics are particularly evident for EV1 and EV2, which exhibit elevated supraharmonic content within these frequency bands.
- The 28 kHz emission peak is linked to background distortion, as it appears in the voltage spectrum even without active EV charging, indicating a grid-originated source.
- Emissions in the 60–70 kHz range for EV1 and EV2 are attributed to their converter switching frequencies. For both EVs, supraharmonic current emissions decrease with increasing cable length.
- A comparison of EV1 and EV2 shows different converter control strategies: EV1 uses a variable switching frequency (59–68 kHz), while EV2 operates at a fixed 64 kHz. This difference affects the supraharmonic emission spectra in the 60–70 kHz range. Further analysis is presented in Section 6.
- The constant switching frequency of EV2's converter results in emissions that are amplitude-modulated by the fundamental voltage, producing distinct supraharmonic sidebands around the switching frequency and its harmonics. This effect, characteristic of fixed-frequency converters, leads to spectral peaks in the supraharmonic range. With longer cable lengths, frequency-dependent impedance alters the prominence of these components, making sidebands more distinct in the voltage spectrum. Further analysis is provided in Section 6.
- The onboard converters in EV4 and EV5 operate at a constant switching frequency of 6 kHz, while EV3 exhibits its strongest emission at approximately 6.3 kHz. The presence of sidebands around the switching frequency in EV3 may be attributed either to modulation by the fundamental component, as observed in EV2.
- The increased emissions in the 2–10 kHz range for EV1 and EV2 are linked to resonance between the onboard EMI filter and cable impedance. For EV1, this effect intensifies with longer cables, shifting the emission peak from 6.9–9.1 kHz (Z1) to 4.3–5.7 kHz (Z3). The shift is due to an increase in inductive reactance, which lowers the resonant frequency of the filter-cable system.
- A similar trend is observed for EV2, where emissions initially span the range of 3.9–9.5 kHz, but

narrow to 3.9–8.5 kHz with increased cable length. These shifts reinforce the impact of cable-dependent resonance effects on supraharmonic emission behavior in EV charging systems. These variations are corroborated by the corresponding supraharmonic voltage emissions in Fig. 8(b).

The observations from the second charging stage (namely, the CC2 stage for EV1 and the CV stage for EV2 when charging on network impedance Z3) were found to be qualitatively similar to those from the first stage. Therefore, these results are omitted here for brevity.

4 Impact of Cable lengths

A simplified converter model, based on [22] (Ch.5, Pg 119), is shown in Figure 9 to analyze the impact of cable length on current emissions. The model includes an input inductor 'L', with an input voltage 'V_{in}' applied at one terminal and a modulated DC output voltage $S_w * V_{dc}$.at the other, controlled by the converter's switching function. The cable impedance is represented as a lumped element 'Z_c'. This analysis focuses on EV1, tested under identical grid conditions with varying cable lengths (Z1, Z2, Z3) as described in Section 2. Grid parameters such as transformer impedance, short circuit impedance at PCC, and remote loads are assumed to be constant, isolating the influence of cable impedance on emission characteristics.

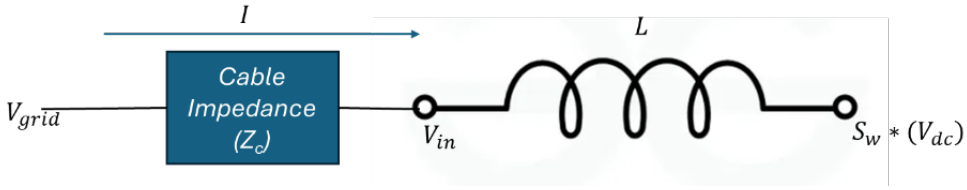

Figure 9 Simplified converter model for studying the impact of cable lengths on current emissions from the converter.

The current sourced by the converter in this case can be derived using Eq.1 [22] (Ch. 5, Pg 120), and the background grid voltage can be derived using Eq.2.

$$I = ((V_{in}) - S_w * (V_{dc}))/((\omega * L) + Z\_c) \quad (1)$$

$$V_{grid} = V_{in} + I * Z_c \quad (2)$$

In the frequency range below 2 kHz, where the cable impedance is assumed to be inductive, as the cable's inductive reactance increases with frequency, the impedance presented to the converter rises, resulting in reduced current injection. This leads to lower emission levels. However, due to the frequency-dependent voltage drop across the cable, an increase in background voltage distortion is expected, particularly at harmonic frequencies where the cable reactance is significant.

The model is validated using EV1 measurements by comparing the mean, 95th percentile, and peak current emissions across different grid impedances. Figure 10 presents these variations for interharmonic (a), harmonic (b), and supraharmonic (c) frequency ranges, along with corresponding voltage distortion. Only Phase A results are shown for brevity. In the bar plots, a positive difference in current emissions indicates agreement with the model, i.e., emissions decrease with higher impedance, while a negative difference signals deviation. For voltage, a negative difference reflects model compliance, indicating increased distortion with rising impedance; a positive difference suggests the opposite.

From Fig. 10 (a) for interharmonic emissions, statistically significant deviations are observed at interharmonic orders 0 and 1 when EV1 is charging under grid impedance conditions Z2 and Z3. This deviation is associated with a comparatively higher fundamental current: the difference in mean charging current between Z1 and Z2 is -0.12 A, while for Z1 and Z2 it reaches -0.5 A. Similarly, the mean difference in terminal voltage at the fundamental frequency is 5.3 V between Z1 and Z2, and 7.2 V between Z1 and Z3. From Fig. 10(b), statistically significant deviations are observed for the triplen harmonics as well as for harmonic orders 11 and 13. These deviations may be attributed to the specific converter or controller architecture employed in the EV. For instance, converter topologies such as the Vienna rectifier commonly utilize third harmonic injection techniques to balance the neutral point voltage [23],[24]. This could provide a plausible explanation for the observed deviations in triplen harmonic emissions. Additionally, the presence of elevated 11th and 13th harmonics may be linked to changes in background voltage distortion. Further analysis on the behavior of the different converter architectures will be undertaken as part of a separate publication. Figure 10(c) illustrates the deviations observed in the supraharmonic frequency range. These deviations are likely attributable to resonance phenomena identified in Figure 8, which can amplify specific frequency components depending on the grid impedance and system configuration. The resonance effects contribute to the non-compliance with the expected emission trends under varying impedance conditions.

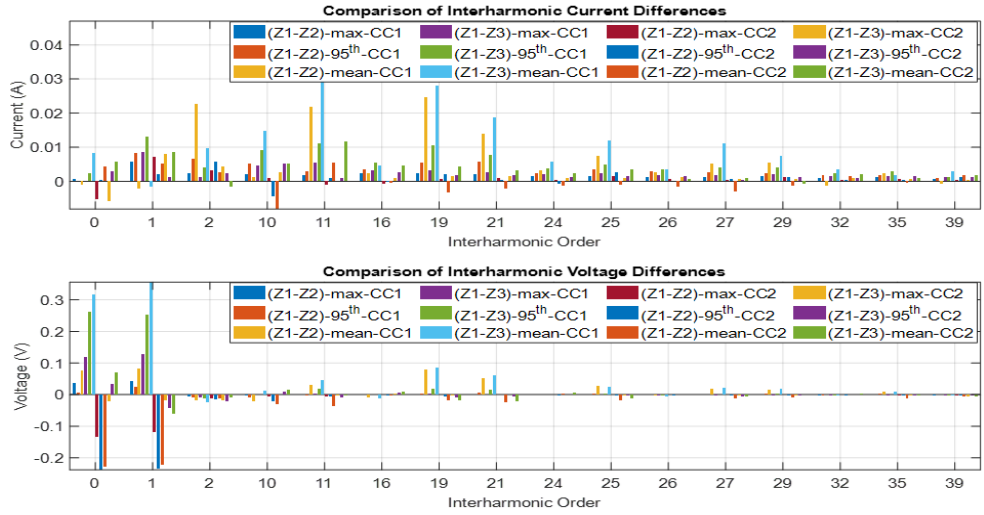

(a)

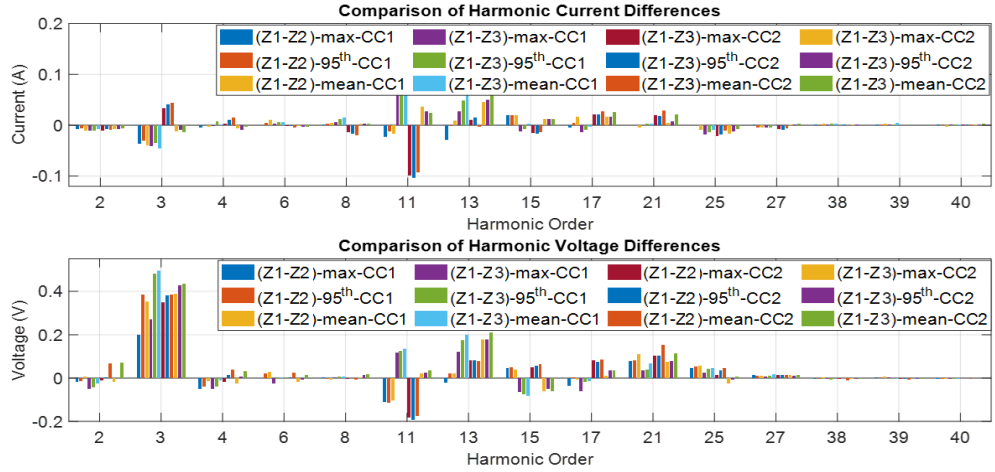

(b)

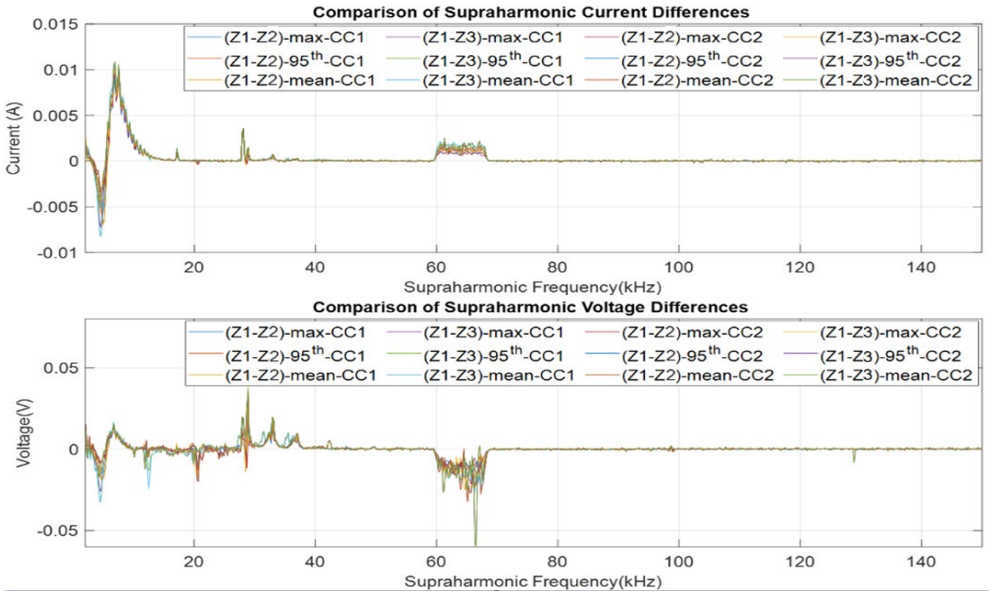

(c)

Figure 10: Comparison of converter current distortion (mean, 95th percentile, peak) under varying grid impedances for (a) interharmonic, (b) harmonic, and (c) supraharmonic ranges. Highlighted cases show deviations from expected trends and corresponding voltage distortion.

5 Impact of background voltage distortion in the supraharmonic frequency range (9-150 kHz range)

The analysis of supraharmonic emissions as a percentage of the emission limits in Section 4.3 demonstrated the influence of cable impedance on the magnitude and distribution of supraharmonic components. Consequently, certain frequency components present in the EV emission spectra were not previously highlighted or discussed in detail. In this section, the novel light Quasi-Peak (QP) method, as proposed in [25], is employed to extract the quasi-peak values of EV emissions in the 9-150 kHz frequency range. The measured emissions are assessed against the limits specified in IEC 61000-2-2 for supraharmonic voltages and Section II of the standard for supraharmonic currents. The resulting three-phase quasi-peak supraharmonic voltages and currents for EV1 and EV2 during charging are illustrated in Figure 11. Key conclusions based on the observed supraharmonic spectrum in Figure 11 are presented below.

- In the switching frequency range (59–68 kHz for EV1 and 64 kHz for EV2), the magnitudes of supraharmonic current and voltage emissions in phase A are consistently lower than those observed in phases B and C. This discrepancy may be attributed to differences in the grid impedance seen by phase A. One potential contributor to this variation is the EVSE, whose controller (responsible for managing communication between the EVSE and the EV) draws current exclusively from phase A, thereby affecting its impedance characteristics.
  A distinct background distortion component at 28 kHz is consistently observed in the supraharmonic current and voltage spectra for both EV1 and EV2, indicating the presence of a persistent disturbance in this frequency range.
- Additional spectral components are observed in the 30–40 kHz range within both the voltage and current spectra of EV1 and EV2. While the exact origin of these distortions remains unidentified, potential sources are discussed to provide plausible explanations for their occurrence.

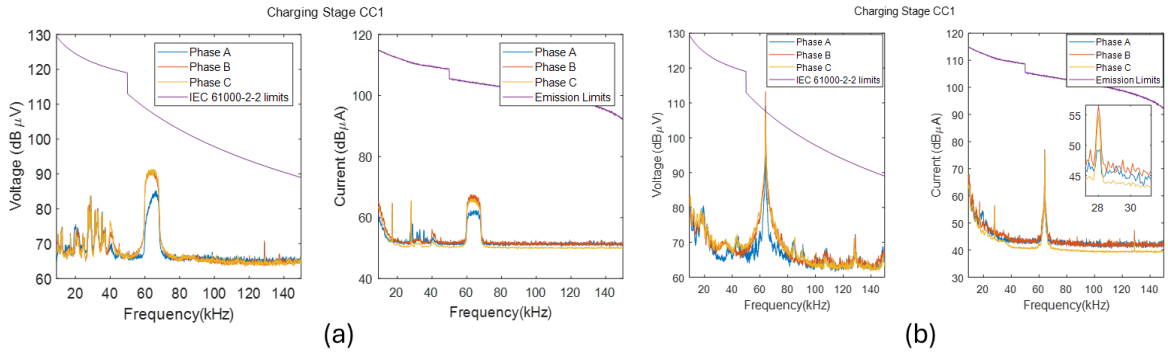

Figure 11: Quasi Peak (QP) values of supraharmonic voltage and current emissions from EV charging: (a) EV1, (b) EV2

The time–frequency representation of the supraharmonic spectrum of EV1 is presented in the form of a spectrogram in Fig.12, enabling visualization of the temporal evolution and persistence of specific frequency components during the EV charging process. Fig.12(a) shows the spectrogram of the background supraharmonic voltage without an EVSE or an EV connected to the grid. A 28 kHz supraharmonic constant frequency distortion is observed in phase B alone as part of the background distortion. With the EVSE connected and EV1 charging with a network impedance of Z1, the 28 kHz component is also visible on phases A (not shown) and C. The spectrogram of the phase voltages and EV charging current is shown in Fig.12(b), and it shows the 28 kHz component. The following two reasons can explain the presence of the 28 kHz component in phases A and C:

- The presence of an ‘X’ capacitor between phase B and phase A and between phase B and phase C in the input filter of the EV provides a conductive path for the 28 kHz component to couple with the other phases.
- The 28 kHz component is assumed to be conducted to the DC side of the converter through the semiconductor switches, which exhibit capacitive behavior at high frequencies. This high-frequency ripple may originate from two possible mechanisms: (i) conduction of the 28 kHz disturbance from the AC side, or (ii) intrinsic ripple generated on the DC side by the operation of a backend DC–DC converter that regulates the terminal voltage at the battery. This ripple is subsequently coupled back into the AC grid voltages via modulation by the converter’s PWM switching function. A detailed mathematical description of this coupling mechanism is provided in [22] (Ch5,Pg 155).

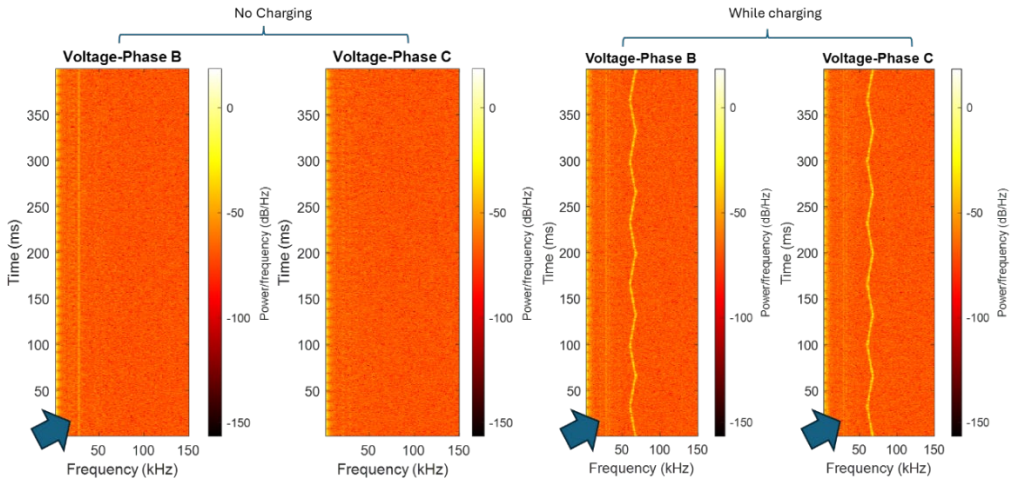

Figure 12: (a)Spectrogram of no-load voltage of Phase B and C. The 28 kHz distortion is highlighted on Phase B with an arrow. (b) Spectrogram of the voltage waveform of Phase B and C while charging, showing the 28 kHz distortion and time varying switching frequency distortion present on both phases B and C.

The spectrogram of the input voltages on phases B and C during EV charging, shown in Figure 12(b), reveals that EV1 employs a variable switching frequency PWM (VSFPWM) scheme with a triangular frequency sweep profile and a period of approximately 65 msec. The use of VSFPWM offers several advantages, including reduced switching losses, lower current and voltage ripple, and improved electromagnetic interference (EMI) performance, as discussed in [26],[27], and [28]. The interaction between the constant 28 kHz background disturbance and the variable switching frequency (ranging from 58 kHz to 68 kHz) may result in modulation sidebands. These sidebands occur at frequencies that the intermodulation relationship gives in Eq.(3).

$$f_{intermodulation} = n * f_{sw} \pm m * f_{dist} \quad (3)$$

where $f_{sw}$is the switching frequency, f_{dist} is the disturbance frequency (28 kHz), and m, n are integers. For the lower end of the sweep, sidebands may appear at 30 kHz and 86 kHz (58 ± 28 kHz), and for the upper end, at 40 kHz and 96 kHz (68 ± 28 kHz). These components are indicative of intermodulation between the background distortion and the converter's switching behavior.

This phenomenon is verified by extending the simplified converter model introduced in Section 5, wherein a 28 kHz disturbance is introduced on the DC side. The DC bus voltage is assumed to be 400 V. The switching function employed is a rectangular pulse train with a 50% duty cycle, whose frequency is linearly swept from 58 kHz to 68 kHz over a period of 32.5 ms, and then back to 58 kHz, forming a triangular frequency modulation profile. The converter's input filter includes a 20 mH inductor. The input to this inductor is a 230 V sinusoidal voltage source superimposed with a 28 kHz disturbance of 1 V magnitude. The Fast Fourier Transform (FFT) of the resulting current waveform is shown in Figure 13, illustrating the interaction between the injected disturbance and the variable switching frequency of the converter.

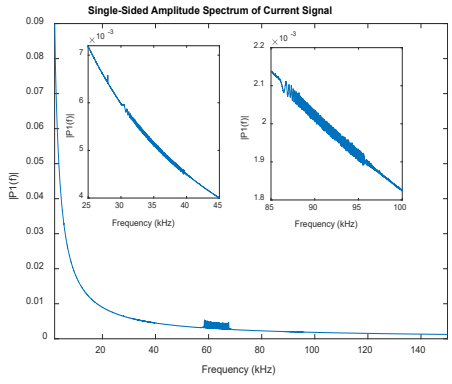

Figure 13 Single side FFT of the converter current with a simulated condition of a constant frequency 28 kHz disturbance on the AC grid and conducted on to the DC side of the EV front-end converter operating with a variable switching frequency pulse width modulated (VSFPWM).

These results offer a plausible explanation for the additional spectral components observed in Figure 11(a). However, conclusive validation of the proposed model would require direct measurements on both the AC and

DC sides of the converter, an approach that is not feasible in commercially available EVs due to limited access to internal power electronic interfaces

Conclusions

This paper presents a comprehensive evaluation of waveform distortion caused by five commercially available electric vehicles (EVs) during Mode 3 charging on a low-voltage distribution network. By varying cable lengths, the influence of grid impedance on harmonic, interharmonic, and supraharmonic emissions was systematically studied through both measurements and modeling. A simplified converter model was employed to interpret the impact of cable impedance on current emissions, with validation based on statistical analysis of measured data.

Key findings include the identification of three dominant supraharmonic frequency bands (2–10 kHz, ~28 kHz, and 60–70 kHz), with emissions in the latter range linked to EV converter switching frequencies. In the 60-70 kHz band associated with the converter's switching frequency, emissions in this band were observed to decrease with increased cable length. A persistent 28 kHz component was attributed to background grid distortion rather than EV behavior. In the 2-10 kHz band, differences in emission characteristics were observed due to possible shifts in the resonance frequency of the frequency-dependent network impedance. Differences between EVs were also traced to variations in converter control strategies, such as fixed versus variable switching frequencies.

The use of a light quasi-peak method further enabled a more refined assessment of supraharmonic emissions, benchmarked against applicable limits. Overall, the results underscore the significant influence of grid impedance, background distortion, and converter architecture on EV emission profiles. These insights are critical for improving grid compatibility assessments and guiding future updates to emission standards for electric vehicle charging.

References

[1] S. Bouckaert *et al.*, “Net zero by 2050: A roadmap for the global energy sector,” 2021.

[2] Anette Myhr, “Vehicle Statistics (Sweden 2024),” 2024. Accessed: Apr. 18, 2025. [Online]. Available: https://www.trafa.se/en/road-traffic/vehicle-statistics/

[3] A. J. Collin *et al.*, “Survey of harmonic emission of electrical vehicle chargers in the European market,” in *2016 International Symposium on Power Electronics, Electrical Drives, Automation and Motion (SPEEDAM)*, 2016, pp. 1208–1213. doi: 10.1109/SPEEDAM.2016.7526005.

[4] S. Sudha Letha and M. Bollen, “Impact of Electric Vehicle Charging on The Power Grid,” 2021.

[5] M. H. Bollen, “Overview of Power Quality and Power Quality Standards,” in *Understanding Power Quality Problems: Voltage Sags and Interruptions*, 2000, pp. 1–34. doi: 10.1109/9780470546840.ch1.

[6] A. Bracale *et al.*, “Harmonic and Supra-Harmonic Emissions of Electric Vehicle Chargers: Modeling and Cumulative Impact Indices,” *IEEE Open Access Journal of Power and Energy*, vol. 11, pp. 690–702, 2024, doi: 10.1109/OAJPE.2024.3521030.

[7] M. Huang, S. Huang, and J. Jiang, “Harmonic study of electric vehicle chargers,” *Beijing Jiaotong Daxue Xuebao/Journal of Beijing Jiaotong University*, vol. 32, no. 5, pp. 85–88, Oct. 2008, doi: 10.1109/icems.2005.203002.

[8] G. Foskolos, “Measurement-based current-harmonics modeling of aggregated electric-vehicle loads using power-exponential functions,” *World Electric Vehicle Journal*, vol. 11, no. 3, Sep. 2020, doi: 10.3390/WEVJ11030051.

[9] T. Slangen, “Supraharmonics and Electric Vehicle Charging: Study on Emission, Summation and Propagation of Conducted Disturbances in the Frequency Range 2-150 kHz,” 2023.

[10] T. Slangen, T. van Wijk, V. Ćuk, and S. Cobben, “The propagation and interaction of supraharmonics from electric vehicle chargers in a low-voltage grid,” *Energies (Basel)*, vol. 13, no. 15, Aug. 2020, doi: 10.3390/en13153865.

[11] L. Wang, Z. Qin, T. Slangen, P. Bauer, and T. van Wijk, “Grid Impact of Electric Vehicle Fast Charging Stations: Trends, Standards, Issues and Mitigation Measures - An Overview,” *IEEE Open Journal of Power Electronics*, vol. 2, pp. 56–74, Jan. 2021, doi: 10.1109/ojpel.2021.3054601.

[12] V. Erhan, T. M. H. Slangen, V. Cuk, J. F. G. Cobben, and T. Van Wijk, “Measurement and Analysis of the Low Voltage Network Impedance in the Supraharmonic Range,” in *Proceedings of International Conference on Harmonics and Quality of Power, ICHQP*, IEEE Computer Society, 2022. doi: 10.1109/ICHQP53011.2022.9808479.

[13] “Electric vehicle conductive charging system-Part 1: General requirements IEC 61851-1,” 2017, [Online]. Available: https://webstore.iec.ch/publication/33644

[14] International Electrotechnical Commission. and International Electrotechnical Commission., *Electric vehicle conductive charging system. P. 21-2, Electric vehicle requirements for conductive connection to an AC/DC supply - EMC requirements for off-board electic vehicle charging systems IEC 61851-21-2*. IEC, 2018.

[15] *Electromagnetic compatibility (EMC) – Part 3-2: Limits – Limits for harmonic current emissions (equipment input current ≤ 16 A per phase) AS IEC 61000-3-2*.
[16] "IEC 61000-3-12, Electromagnetic compatibility (EMC) – Part 3-12: Limits – Limits for harmonic currents produced by equipment connected to public low-voltage systems with input current >16 A and <75 A per phase," 2011.
[17] *Electromagnetic compatibility (EMC) Part 2-2: Environment Compatibility levels for low frequency conducted disturbances and signalling in public low-voltage power supply systems AS IEC 61000-2-2*. 2018. [Online]. Available: www.iec.ch/catlg-f.htm
[18] EMC & Power Quality (D-A-CH-CZ), "Technical rules for the assessment of network disturbance Part A: Fundamentals," 2021.
[19] EMC & Power Quality (D-A-CH-CZ), "Technical Rules for the assessment of network disturbance Part B: Requirements and assessment Section I : Low voltage," 2021.
[20] IEC, *Electromagnetic compatibility (EMC) - Part 4-7: Testing and measurement techniques - General guide on harmonics and interharmonics measurements and instrumentation, for power supply systems and equipment connected thereto*. 2002.
[21] IEC, *Electromagnetic compatibility (EMC) - Part 3-14: Assessment of emission limits for harmonics, interharmonics, voltage fluctuations and unbalance for the connection of disturbing installations to LV power systems*. 2011.
[22] A. Yazdani and R. Iravani, *Voltage-sourced converters in power systems: modeling, control, and applications*. John Wiley & Sons, 2010.
[23] D. A. Molligoda *et al.*, "Current Distortion Mitigation in Grid-Connected Vienna Rectifier During Nonunity Power Factor Operation," in *IECON 2020 The 46th Annual Conference of the IEEE Industrial Electronics Society*, 2020, pp. 4085–4090. doi: 10.1109/IECON43393.2020.9255341.
[24] J.-H. Park, J.-S. Lee, and K.-B. Lee, "Sinusoidal Harmonic Voltage Injection PWM Method for Vienna Rectifier With an LCL Filter," *IEEE Trans Power Electron*, vol. 36, no. 3, pp. 2875–2888, 2021, doi: 10.1109/TPEL.2020.3011435.
[25] A. Gallarreta *et al.*, "A Light Measurement Method for 9–150 kHz Disturbances in Power Grids Comparable to CISPR Quasi-Peak," *IEEE Trans Instrum Meas*, vol. 71, pp. 1–10, 2022, doi: 10.1109/TIM.2022.3195255.
[26] Y. Wu, J. Xu, T. B. Soeiro, P. Bauer, and Z. Qin, "Frequency Design of Three-phase Active Front-End Converter with Reduced Filter in EV Chargers," *IEEE Transactions on Transportation Electrification*, p. 1, 2024, doi: 10.1109/TTE.2024.3381167.
[27] M. Haider *et al.*, "Novel ZVS S-TCM Modulation of Three-Phase AC/DC Converters," *IEEE Open Journal of Power Electronics*, vol. 1, pp. 529–543, 2020, doi: 10.1109/OJPEL.2020.3040036.
[28] D. Rothmund, T. Guillod, D. Bortis, and J. W. Kolar, "99.1% Efficient 10 kV SiC-Based Medium-Voltage ZVS Bidirectional Single-Phase PFC AC/DC Stage," *IEEE J Emerg Sel Top Power Electron*, vol. 7, no. 2, pp. 779–797, 2019, doi: 10.1109/JESTPE.2018.2886140.

Presenter Biography

Manav Giri (Graduate Student Member, IEEE) is currently pursuing a Ph.D. degree with the Electric Power Engineering Group at Luleå University of Technology, Skellefteå, Sweden. He is researching waveform distortion in LV networks from Electric Vehicle Charging

Sarah K. Rönnberg (SM'18) obtained her Ph.D. in electric power engineering from Luleå University of Technology, Sweden in 2013. She is currently a Professor with the Department of Engineering Sciences and Mathematics at the same university. Her research interests include supraharmonics, power system harmonics and power quality in general.